

CERN-TH/2003-066

LPT Orsay 03-21

UCOFIS 2/03

April 2003

Nuclear Structure Functions at Small x from Inelastic Shadowing and Diffraction

N. Armesto^{a,1}, A. Capella^{b,2}, A. B. Kaidalov^{c,3},
J. López-Albacete^{a,d,4} and C. A. Salgado^{a,5}

^a *Theory Division, CERN, CH-1211 Genève 23, Switzerland*

^b *Laboratoire de Physique Théorique, Université de Paris XI, Bâtiment 210,
F-91405 Orsay Cedex, France*

^c *Institute of Theoretical and Experimental Physics, B. Cheremushkinskaya 25,
Moscow 117259, Russia*

^d *Departamento de Física, Módulo C2, Planta baja, Campus de Rabanales,
Universidad de Córdoba, 14071 Córdoba, Spain*

Nuclear structure functions at small x and small or moderate Q^2 are studied using the relation with diffraction on nucleons which arises from Gribov's Reggeon Calculus. A reasonable description of experimental data is obtained with no fitted parameters. A comparison with other models and predictions for future lepton-ion colliders are provided. Consequences for the reduction of multiplicities in nucleus-nucleus collisions at energies of RHIC and LHC are examined.

¹ E-mail: Nestor.Armesto.Perez@cern.ch

² E-mail: Alphonse.Capella@th.u-psud.fr

³ E-mail: kaidalov@heron.itep.ru

⁴ E-mail: Javier.Lopez.Albacete@cern.ch

⁵ E-mail: Carlos.Salgado@cern.ch

1 Introduction

The study of nuclear structure functions has become a fashionable subject. Apart from its intrinsic interest, such analysis has a great impact on the interpretation of results from heavy ion experiment. At small values of the Bjorken variable x ($\lesssim 0.01$, shadowing region), the structure function F_2 per nucleon turns out to be smaller in nuclei than in a free nucleon [1, 2]. Several explanations to this shadowing have been proposed.

On the one hand, some models use the fact that, in the rest frame of the nucleus the incoming photon splits into a $q\bar{q}$ pair long before reaching the nucleus, and this $q\bar{q}$ pair interacts with it with typical hadronic cross sections, which results in absorption [3, 4, 5, 6, 7, 8, 9]. Thus nuclear shadowing is a consequence of multiple scattering which in turn is related to diffraction [6, 10, 11]. This relationship will be developed in this paper. Equivalently, in a frame in which the nucleus is moving fast, gluon recombination due to the overlap of the gluon clouds from different nucleons reduces the gluon density in the nucleus [12, 13]. These studies have received great theoretical impulse with the development of semiclassical ideas in QCD and the appearance of non-linear equations for evolution in x in this framework (see [14, 15, 16, 17] and references therein; also [18] for a simple geometrical approach in this framework).

On the other hand, other approaches [19, 20, 21] do not address the origin of shadowing but only its evolution with $\ln Q^2$: parton densities inside the nucleus are parametrized at some scale Q_0^2 and then evolved using the DGLAP [22] evolution equations.

The results from different models usually depend on phenomenological assumptions and their predictions (notably for small values of x which are of uttermost importance to compute particle production at RHIC and LHC) turn out to be very different. For example, concerning the Q^2 -dependence of shadowing, it can be either constant [4, 5, 6, 7, 8, 9], or die out logarithmically [19, 20, 21] or behave as a higher-twist [12, 13].

In this paper we will use the relation of diffraction to nuclear shadowing which arises from Gribov Theory [23], Reggeon Calculus [24] and the AGK rules [25]. In this way we obtain a parameter-free description of nuclear structure functions in the shadowing region valid for $x < 0.01$ and $Q^2 < 10$ GeV 2 , using a model for F_2 and

F_{2D} [26, 27]. The same strategy has been used in [10, 11], but our extrapolation to smaller x or higher W^2 is more reliable than that of [10] due to the model employed for the nucleon; besides, our description is valid for small Q^2 while that of [11] applies to $Q^2 \geq 4 \text{ GeV}^2$. In Section 2 the model will be described. In Section 3 numerical results will be presented together with comparisons with experimental data and with other models. In Section 4 the model will be applied to calculate the multiplicity reduction factors [28, 29] relevant to compute particle production in heavy ion collisions at RHIC and LHC. Finally, the last Section will contain our conclusions.

2 Description of the model

We assume that nuclei are made of nucleons in the spirit of the Glauber model. In order to relate diffraction on nucleons with nuclear shadowing, we will follow the procedure explained in [10]. The γ^* -nucleus cross section can be expanded in a multiple scattering series containing the contribution from 1, 2, ... scatterings:

$$\sigma_A = \sigma_A^{(1)} + \sigma_A^{(2)} + \dots \quad (1)$$

$\sigma_A^{(1)}$ is simply equal to $A\sigma_{\text{nucleon}}$. Let us consider now the first correction to the non-additivity of cross sections which comes from the second-order rescattering $\sigma_A^{(2)}$. In Fig. 1 diffractive DIS is shown in both the infinite momentum frame and in the rest frame of the nucleon. In Fig. 2 it becomes clear that the square of such contribution is equivalent to a double exchange with a cut between the exchanged amplitudes, a so-called diffractive cut. To compute the first contribution to nuclear shadowing $\sigma_A^{(2)}$, which comes from these two exchanges, we need its total contribution to the γ^* -nucleon cross section, which arises from cutting the two-exchange amplitude in all possible ways (between the amplitudes and the amplitudes themselves in all possible manners). For purely imaginary amplitudes, it can be shown [24, 25] that this total contribution is identical to minus the contribution from the diffractive cut. Thus diffractive DIS is directly related to the first contribution to nuclear shadowing. The final expression reads

$$\sigma_A^{(2)} = -4\pi A(A-1) \int d^2b T_A^2(b) \int_{M_{min}^2}^{M_{max}^2} dM^2 \left. \frac{d\sigma_{\gamma^* p}^D}{dM^2 dt} \right|_{t=0} F_A^2(t_{min}), \quad (2)$$

with $T_A(b) = \int_{-\infty}^{+\infty} dz \rho_A(\vec{b}, z)$ the nuclear profile function normalized to 1, $\int d^2b T_A(\vec{b}) = 1$, and M^2 the mass of the diffractively produced system. The usual variables for

diffractive DIS: Q^2 , x , M^2 and t , or $x_P = x/\beta$, $\beta = \frac{Q^2}{Q^2 + M^2}$, are shown in Fig. 1.

Coherence effects, i.e. the coherence length of the $q\bar{q}$ fluctuation of the incoming virtual photon, is taken into account through

$$F_A(t_{min}) = \int d^2b J_0(b\sqrt{-t_{min}}) T_A(b), \quad (3)$$

with $t_{min} = -m_N^2 x_P^2$ and m_N the nucleon mass. This function is equal to 1 at $x \rightarrow 0$ and decreases with increasing x due to the loss of coherence for $x > x_{crit} \sim (m_N R_A)^{-1}$.

Let us briefly examine (2). Here the real part of the Pomeron amplitude, which is small for the value of the intercept which will be used [27], $\Delta = \alpha_P(t=0) - 1 = 0.2$, has not been taken into account. Also it has been deduced under the approximation $R_A^2 \gg R_N^2$, so the t -dependence of the γ^* -nucleon cross section has been neglected.

For $A > 20$ a nuclear density in the form of a 3-parameter Fermi distribution with parameters taken from [30] will be employed to compute both $T_A(b)$ and (3). For $2 < A \leq 20$ a Gaussian profile function is used [31]:

$$T_A(b) = \frac{3}{2\pi R_A^2} \exp\left(-\frac{3b^2}{2R_A^2}\right), \quad R_A = 0.82A^{1/3} + 0.58 \text{ fm}, \quad (4)$$

but, in order to take into account the t -dependence for these light nuclei, we make in the computation of form factors (3) the substitution

$$R_A^2 \longrightarrow R_A^2 + R_N^2, \quad R_N = 0.8 \text{ fm}. \quad (5)$$

Finally, for deuteron the double rescattering contribution has the form

$$\sigma_A^{(2)} = -2 \int_{-\infty}^{t_{min}} dt \int_{M_{min}^2}^{M_{max}^2} dM^2 \left. \frac{d\sigma_{\gamma^* \text{nucleon}}^D}{dM^2 dt} \right|_{t=0} F_D(t), \quad (6)$$

where $F_D(t) = e^{at}$, $a = 40 \text{ GeV}^{-2}$.

The lower integration limit in (2) and (6) is $M_{min}^2 = 4m_\pi^2 = 0.08 \text{ GeV}^2$, while the upper one is taken from the condition:

$$x_P = x \left(\frac{M^2 + Q^2}{Q^2} \right) \leq x_{Pmax} \implies M_{max}^2 = Q^2 \left(\frac{x_{Pmax}}{x} - 1 \right), \quad (7)$$

with $x_{Pmax} = 0.1$; this value was used in [27] motivated by the fact that the model is only valid for $M^2 \ll W^2$ or $x_P \ll 1$, i.e. a large rapidity gap is required. In our case, variations of x_{Pmax} by a factor 2 do not affect the description of nuclear shadowing at

$x < 0.01$ but the choice $x_{Pmax} = 0.1$ is convenient as it guarantees the disappearance of nuclear shadowing at $x \sim 0.1$ (see below) as in the experimental data.

The relation between $\frac{d\sigma_{\gamma^* p}^D}{dM^2 dt} \Big|_{t=0}$ and $x_P F_{2D}^{(3)}(Q^2, x_P, \beta)$ is provided by the model [27]:

$$\begin{aligned} x_P F_{2D}^{(3)}(Q^2, x_P, \beta) &= x_P \frac{Q^2}{4\pi^2 \alpha_{em}} \int_{-\infty}^0 dt \frac{d\sigma_{\gamma^* p}^D(Q^2, x_P, \beta, t)}{dx_P dt} \\ \implies \frac{d\sigma_{\gamma^* p}^D(Q^2, x_P, \beta)}{dM^2 dt} \Big|_{t=0} &= \frac{4\pi^2 \alpha_{em} B}{Q^2(Q^2 + M^2)} x_P F_{2D}^{(3)}(Q^2, x_P, \beta), \end{aligned} \quad (8)$$

where the usual factorization has been assumed:

$$\frac{d\sigma_{\gamma^* p}^D(x, Q^2, M^2, t)}{dM^2 dt} = \frac{d\sigma_{\gamma^* p}^D(x, Q^2, M^2)}{dM^2 dt} \Big|_{t=0} e^{Bt}, \quad (9)$$

with $B = 6 \text{ GeV}^{-2}$ (as in [32], see the discussion there; this value is slightly smaller than the experimental values $7.2 \pm 1.1(\text{stat.})^{+0.7}_{-0.9}(\text{syst.}) \text{ GeV}^{-2}$ [33] at $\langle Q^2 \rangle = 8 \text{ GeV}^2$ and $6.8 \pm 0.9(\text{stat.})^{+1.2}_{-1.1}(\text{syst.}) \text{ GeV}^{-2}$ [34] for photoproduction). Note that $\frac{d\sigma_{\gamma^* p}^D(x, Q^2, M^2)}{dM^2 dt} \Big|_{t=0}$ can be obtained directly from σ_{tot} . However, the model for diffraction we are using [27] has mainly been tested after integration in t (most available data are integrated in t). For this reason, we use the integrated expression together with the experimental value of B . While this is legitimate at present values of x , it can lead to an underestimation of shadowing at very small x , due to the increase of B with energy¹.

The model in [27] is based on the dipole picture of the photon and contains two components. The small-distance (S) component corresponds to transverse distances r between the q and the \bar{q} of the dipole such that $r < r_0$, and the large-distance (L) component to $r > r_0$, with $r_0 = 0.2 \text{ fm}$. In each component a quasi-eikonal iteration is introduced in order to enforce unitarity. Reggeon and Pomeron exchanges are allowed. For diffraction, a third component is used, namely a contribution from the triple interaction of Reggeons and Pomerons. This model has been designed to describe the small $x < 10^{-2}$, small or moderate $Q^2 < 10 \text{ GeV}^2$ region, and it contains the basic ingredients which allow its safe extrapolation² to very small x or high W^2 .

Eq. (2) corresponds to the case with only two scatterings. Its extension to include higher order rescatterings is model-dependent. We will use two models: a Schwimmer

¹Nevertheless, the effect is not too large: we have checked that an increase of B from 6 to 7.2 GeV^{-2} produces an increase of shadowing for Pb of at most 10 % at $x = 10^{-7}$. As estimates indicate an increase $\lesssim 50$ % in B for the smallest x we have studied, $x = 10^{-7}$, the increase of shadowing due to this effect would be at most ~ 25 % for these values of x .

²In order to use the model for larger x , $0.01 < x < 0.1$, we have made some modifications in [27]: there, in Eq. (26) β_{min} in the normalization denominators has been set to 0, and in Eq. (25) the

unitarization [35] which is obtained from a summation of fan diagrams with triple Pomeron interactions,

$$\sigma_{\gamma^* A}^{Sch} = \sigma_{\gamma^* \text{nucleon}} \int d^2 b \frac{AT_A(b)}{1 + (A-1)f(x, Q^2)T_A(b)} , \quad (10)$$

and an eikonal unitarization,

$$\sigma_{\gamma^* A}^{eik} = \sigma_{\gamma^* \text{nucleon}} \int d^2 b \frac{A}{2(A-1)f(x, Q^2)} \left\{ 1 - \exp \left[-2(A-1)T_A(b)f(x, Q^2) \right] \right\} , \quad (11)$$

where we use the relation $\sigma_{\gamma^* \text{nucleon}} = \frac{4\pi^2 \alpha_{em}}{Q^2} F_2(x, Q^2)$ valid at small x . Here, $F_2(x, Q^2)$ is the nucleon structure function, taken from [27]. Both expressions (10) and (11), expanded to the first non-trivial order, reproduce the second rescattering result (2). Eikonal unitarization will produce larger shadowing than Schwimmer, as can be expected by comparing the second non-trivial order in the expansion of both expressions. Finally,

$$f(x, Q^2) = \frac{4\pi}{\sigma_{\gamma^* \text{nucleon}}} \int_{M_{min}^2}^{M_{max}^2} dM^2 \left. \frac{d\sigma_{\gamma^* p}^D}{dM^2 dt} \right|_{t=0} F_A^2(t_{min}) \quad (12)$$

as required by consistency with (2).

The shadowing in nuclei is usually studied through the ratios of cross sections per nucleon for different nuclei, defined as

$$R(A/B) = \frac{B}{A} \frac{\sigma_{\gamma^* A}}{\sigma_{\gamma^* B}} . \quad (13)$$

In the simplest case of the ratio over nucleon (equivalent to proton at small x where the valence contribution can be neglected), we get:

$$R^{Sch}(A/\text{nucleon}) = \int d^2 b \frac{T_A(b)}{1 + (A-1)f(x, Q^2)T_A(b)} , \quad (14)$$

$$R^{eik}(A/\text{nucleon}) = \int d^2 b \frac{1}{2(A-1)f(x, Q^2)} \left\{ 1 - \exp \left[-2(A-1)T_A(b)f(x, Q^2) \right] \right\} . \quad (15)$$

To calculate shadowing in photoproduction, x is no longer a relevant kinematical variable. Instead we use the γ^* -nucleon center of mass energy W^2 .

In our framework shadowing can also be studied as a function of the impact parameter b :

$$R(A/\text{nucleon})^{Sch}(b) = \frac{1}{1 + (A-1)f(x, Q^2)T_A(b)} , \quad (16)$$

Reggeon-Reggeon contribution has been ignored. These two changes slightly modify the description of diffraction but we have checked that the agreement with experimental data is as good as in the original version of the model.

$$R(A/\text{nucleon})^{eik}(b) = \frac{1}{2(A-1)T_A(b)f(x, Q^2)} \left\{ 1 - \exp \left[-2(A-1)T_A(b)f(x, Q^2) \right] \right\}. \quad (17)$$

Finally, the region of applicability of our model is the same as that of the model for diffraction on nucleon [27], i.e. small $x \lesssim 0.01$ and small or moderate $Q^2 \lesssim 10 \text{ GeV}^2$, including photoproduction.

3 Numerical results

In our model and in [27] we work in the small x region and thus no distinction is made between protons and neutrons. Although usually joined with straight lines, our results are computed at the same $\langle x \rangle$ and $\langle Q^2 \rangle$ as the experimental data. For the latter, inner error bars show statistical errors, and outer error bars correspond to statistical and systematical errors added in quadrature.

In Figs. 3-6 a comparison with experimental data at small x from E665 [36, 37] and NMC [38, 39, 40] is presented. As expected, eikonal unitarization produces larger shadowing than Schwimmer. The agreement with experimental data is quite reasonable taking into account that no parameters have been fitted to reproduce the data. Two comments are in order: First, for C/D and Ca/D in Fig. 3 which shows the comparison with E665 data, shadowing looks overestimated for $x \sim 0.01$, while in Fig. 5 which shows the comparison with NMC data, it looks underestimated. This corresponds to the known difference between the results of both experiments for ratios over D, while the compatibility is restored [38] when ratios are computed over C. Second, from Fig. 6 it becomes clear that the evolution with Q^2 in the model is too slow at $x \sim 0.01$, a problem related with the lack of DGLAP evolution in the model [27] (see [10, 11, 41] for an application of DGLAP evolution to initial conditions).

In Fig. 7 a comparison of the results of our model with those of others is shown, for $Q^2 = 3 \text{ GeV}^2$ (except the results of [11] which are at $Q^2 = 4 \text{ GeV}^2$). It can be seen that the results of different models agree within 15 % at $x \sim 0.01$ where experimental data exist, while they differ up to a factor 0.6 at $x = 10^{-5}$. At this x , our results are the lowest ones but roughly agree with those of [19] and with one set of [11], while the results from [21] are the highest ones, and those of [8, 42, 43] and the second set of [11] lie in between. Let us briefly comment on these models: In [19, 21] an initial condition

is parameterized at some Q_0^2 and then evolved using DGLAP; the initial condition is fitted from the comparison of the evolved results with experimental data (see [44] for a comparison between these two models). [8] is a model which uses a saturating ansatz for the total γ^* -nucleon cross section in the proton, which is introduced in a Glauber expression for its extension to the nuclear case. In [11] some parameterization of hard diffraction at Q_0^2 , which as in the present work gives nuclear shadowing through Gribov's Reggeon Calculus, is employed; this nuclear shadowing computed at Q_0^2 is used as initial condition for DGLAP evolution. In [42] a Glauber ansatz provides with the initial condition for DGLAP evolution. Finally, in [43] a non-linear equation for small x evolution is numerically solved [45] and used in the nuclear case. In view of the differences at small x among different models, a measurement of F_2 in nuclei with $\sim 10\%$ precision would be a sensitive test to discriminate among them. Lepton-ion colliders [46] could provide with such data.

In Fig. 8 our predictions for the ratios D, He, Li, C, Ca, Sn and Pb over nucleon for $Q^2 = 0.5, 2$ and 5 GeV^2 are given for $x > 10^{-8}$. Let us notice that our model is designed for the small x region and that no antishadowing or any other effects relevant for $x \gtrsim 0.1$ have been introduced. The disappearance of shadowing at $x \sim 0.1$ is a consequence of both the coherence effects in (3) and the vanishing integration domain in (2), see (7). In Fig. 9 results in photoproduction for the same ratios as in Fig. 8 are given for $W^2 < 10^5 \text{ GeV}^2$, together with predictions for the evolution of the ratios C and Pb over nucleon with impact parameter b . Values as low as 0.3 are reached for central Pb/nucleon. This evolution with centrality is very important to compute the corresponding evolution of particle production in nuclear collisions, and could also be measured in lepton-ion colliders [46].

As a last comment in this Section, let us discuss about the twist structure of the model (i.e. its structure in powers of $1/Q^2$). In the model of [27] the unitarity corrections to the L -component are all of order $1/Q^2$. On the contrary, in the S -component the unitarity corrections are higher-twist (they can be expanded as a sum of terms, each one containing an additional factor $1/Q^2$ as compared to the previous one). The fact that diffraction is related to the unitarity corrections allows to study the $1/Q^2$ behavior of shadowing in this model. In order to keep only the leading-twist contribution (terms $\propto 1/Q^2$ in the cross section) we ignore the higher-twist contribution of

the S -component to the diffractive cross section³. The results are given in Fig. 10. One can see that neglecting these terms introduces only a small difference. The fact that nuclear shadowing corrections are predominantly leading-twist is not unexpected, as the diffractive cross section is also leading-twist for the relevant kinematical region (indeed, in the model of [27] the S -component diffraction is almost negligible for small Q^2 and/or large M^2). This is also seen in the fact that the ratio of diffractive to inclusive cross sections does not show any strong Q^2 -dependence for large M^2 [47]. Here a comment is in order: in [27] a parameter s_0 is introduced in x and β to control the limit $Q^2 \rightarrow 0$, so that all the equations are written for $\bar{x} = x + s_0/(W^2 + Q^2)$, $\bar{\beta} = \beta + s_0/(M^2 + Q^2)$. These terms could mimic higher-twist corrections. In Fig. 10 we check that the effect of varying this parameter⁴ from the original $s_0 = 0.79 \text{ GeV}^2$ to $s_0 = 0.2 \text{ GeV}^2$ is also very small. So, we can conclude that the contribution from higher-twist terms to the shadowing of F_2 is small. In contrast, in [11] a large higher-twist correction for the shadowing is claimed. The approach in this reference is very similar to ours: the authors also compute shadowing from the diffractive cross section, but using the H1 parametrization [48]. The shadowing obtained in this way for $Q_0^2 = 4 \text{ GeV}^2$ is then employed as initial condition for DGLAP evolution, taking the shadowing for valence quarks from [19]. When evolved downwards to $Q^2 = 3 \text{ GeV}^2$ a disagreement is found with experimental data on the ratio Ca over D. This disagreement is attributed to higher-twist contributions.

4 Multiplicity reduction in nucleus-nucleus collisions

In this framework it is also possible to study the reduction of multiplicities in nucleus-nucleus collisions [49, 28, 29]. We will denote the rapidity of the produced system in the center of mass frame by y^* . Shadowing as a function of the rapidity of the produced particle can be computed taking into account the general relation with the diffractive variables:

$$y = \ln \left(\frac{1}{x_P} \right) = \ln \left(\frac{s}{M^2} \right). \quad (18)$$

³Concretely, we ignore the S -component in (17) of [27], and in (20) of [27] we set the exponential containing χ_S to 1.

⁴And setting $c = 0$ in Eq. (27) of [27].

Then the factor for reduction of multiplicities at fixed impact parameter b is [49, 28, 29]

$$R_{AB}(b) = \frac{\int d^2s \ R_A(\vec{s})R_B(\vec{b} - \vec{s})}{T_{AB}(b)}. \quad (19)$$

$R_{A(B)}(b)$ is given by the r.h.s. of (16) multiplied by $T_{A(B)}(b)$ and with $f(x, Q^2)$ substituted by $F(s, y^*)$ (see below), and

$$T_{AB}(b) = \int d^2s \ T_A(\vec{s})T_B(\vec{b} - \vec{s}). \quad (20)$$

(19) takes into account the summation of Schwinger's fan-like diagrams for the projectile and target, which are joined by a single Pomeron whose cut gives rise to the produced particle (Fig. 11). It follows from AGK cancellation [25] that this is the only contribution of this type (more complicated diagrams with lines joining upper and lower parts of the diagram, cancel). This provides the justification for the factorized expression (19), which is true even if more general rescattering diagrams are taken into account.

The reduction factor as a function of the rapidity of the produced particles $F(s, y^*)$, can be calculated in several ways. The first one is using (12), but with the integration limits inspired by the parton model for hard processes: for projectile A (target B),

$$x_{A(B)} = \frac{m_T}{\sqrt{s}} e^{\pm y^*}, \quad (21)$$

with $y^* > 0$ for the projectile hemisphere and $y^* < 0$ for the target one, and $m_T = \sqrt{m^2 + p_T^2}$ the transverse mass of the produced particle. Substituting in the general relation for M_{max}^2 , (7), we get

$$M_{max}^{2(A(B))} = Q^2 \left(\frac{x_{Pmax}}{x_{A(B)}} - 1 \right) = Q^2 \left(\frac{x_{Pmax} \sqrt{s}}{m_T} e^{\mp y^*} - 1 \right), \quad (22)$$

while M_{min}^2 remains fixed and equal to 0.08 GeV^2 , and $Q^2 = m_T^2$.

On the other hand, we can also compute the reduction factor from the formulas [28, 29]

$$F(s, y^*) = 4\pi \int_{y_{min}}^{y_{max}} dy \left. \frac{1}{\sigma_P(s)} \frac{d\sigma^{PPP}}{dydt} \right|_{t=0} F_A^2(t_{min}), \quad (23)$$

where $\sigma_P(s)$ is the single Pomeron exchange cross section and $\frac{d\sigma^{PPP}}{dydt}$ the triple Pomeron cross section. Using the standard triple Pomeron formula for the latter, we get

$$\left. \frac{1}{\sigma_P(s)} \frac{d\sigma^{PPP}}{dydt} \right|_{t=0} = C \Delta \exp(\Delta y), \quad (24)$$

with $C = \frac{g_{pp}^P(0)r_{PPP}(0)}{4\Delta}$, $g_{pp}^P(0)$ the Pomeron-proton coupling and $r_{PPP}(0)$ the triple Pomeron coupling, both evaluated at $t = 0$. In this case, the same integration limits used above correspond to:

$$y_{min}^{(A(B))} = \ln \left(\frac{s}{M_{max}^{2(A(B))}} \right), \quad (25)$$

with $M_{max}^{2(A(B))}$ given by (22), and

$$y_{max}^{(A(B))} = \frac{1}{2} \ln \left(\frac{s}{m_T^2} \right) \mp y^*. \quad (26)$$

In the calculations we have used [$C = 0.31 \text{ fm}^2, \Delta = 0.13$] taken from [50] (used in [28, 29]). A value $m_T = 0.4 \text{ GeV}$ is employed by default (in [28, 29] the nucleon mass m_N was used). The sensibility of our results to variations in m_T will be examined.

In Fig. 12 our results at $y^* = 0$ are presented for AuAu at RHIC energies and for PbPb collisions at the LHC, versus impact parameter. Reductions of multiplicities at $b = 0$ by factors $\sim 1/2$ for RHIC and $\sim 1/3$ for LHC are found, with a clear increase of the suppression with increasing energy. In Fig. 13 results are presented for AuAu at RHIC and PbPb at LHC for different y^* . Finally, in Fig. 14 the variation with m_T of the results at $y^* = 0$ for AuAu at RHIC is studied. A reduction of the suppression with increasing m_T is seen, as expected. Let us make two comments: First, our results for the reduction factors are very similar to the ones estimated in [28, 29]. It has been shown in [28, 29] that, when these reduction factors are used to correct the results of the Dual Parton Model, one obtains a good description of the RHIC data on multiplicities and their evolution with centrality. Thus, our results provide a detailed calculation of these reduction factors which confirms the estimations in [28, 29]. Second, our results are important in studying particle production in heavy ion collisions. In particular, the dependence of the reduction factors on m_T gives the variation of shadowing corrections with the p_T of the produced particle⁵.

5 Conclusions

In this paper, we have used the relation which arises from Reggeon Calculus and the AGK rules, between the diffractive cross section measured in DIS on nucleons and the

⁵For reduction factors based on other mechanisms, see [51, 52].

first contribution (i.e. double scattering) to nuclear shadowing. The next contributions have been estimated using two different methods for unitarization. In this way we have obtained a description of nuclear shadowing, based on the model of [27] for diffraction, which agrees with the existing experimental data without any fitted parameter. The model is designed for the region of $x < 0.01$ and $Q^2 < 10 \text{ GeV}^2$, i.e. small x and small or moderate Q^2 .

The same method has been applied in [10, 11]. In [10], a model for diffraction [50] has been used that takes into account unitarization effects in an effective manner, so the extrapolation to smaller x or larger W^2 is not so reliable as in the full unitarization program followed in [27]; furthermore, the description of diffraction in the model we use is substantially better due to the inclusion in the fits of new, more precise experimental data. In [11], a model for diffraction is used in order to obtain an initial condition for DGLAP evolution at $Q_0^2 = 4 \text{ GeV}^2$, so their leading-twist description for nuclear shadowing is not valid at small Q^2 . On the contrary, we develop a model valid for the full low Q^2 region which does not correspond to any definite twist but contains contributions from all twist orders. Nevertheless, it turns out that, as discussed at the end of Section 3, the leading-twist contribution is the dominant one in our model, which is in reasonable agreement with the existing experimental data. Precise data on the Q^2 -dependence of nuclear structure functions should disentangle between these two possibilities. The existing data from NMC [40] can be well reproduced within the leading-twist DGLAP evolution [19] with an appropriate set of initial conditions. An extension of our results using DGLAP evolution for large values of Q^2 is thus a natural continuation of our work [41].

In this framework we have also obtained the factor for multiplicity reduction in nucleus-nucleus collisions. This factor reaches values $\sim 1/2$ and $\sim 1/3$ for central AuAu and PbPb collisions at RHIC and LHC respectively. It is therefore a very important ingredient for the computation of particle production at these energies which should be taken into account together with other possible effects.

Comparison among models shows differences of a factor 0.6 for the ratio of structure functions Pb/nucleon at $x = 10^{-5}$ and $Q^2 = 3 \text{ GeV}^2$. These differences have a large impact in the computation of particle production in nuclear collisions at energies of RHIC and LHC. They should be testable in future lepton-ion colliders [46].

To conclude, the method which we have followed offers a natural link between the measurements of nucleon diffractive structure functions and nuclear shadowing, and between the latter and the suppression of particle production in nuclear collisions. In this way the study of Low x Physics at HERA is linked to that of nuclear structure functions at future lepton-ion colliders and with Heavy Ion Physics at RHIC and LHC [15].

Acknowledgments: The authors express their gratitude to B. Badelek, E. G. Ferreiro, B. Z. Kopeliovich, J. Raufeisen and M. Strikman for useful comments and discussions. They also thank M. Lublinsky for discussions and for providing the results [43], and C. Pajares for a reading of the manuscript. A. C., A. B. K. and C. A. S. acknowledge financial support by grant INTAS 00-00366, and A. B. K. by grants RFBR 00-15-96786, RFBR 01-02-17383 and DFG 436 RUS 113/721/0-1. N. A. thanks the Institute for Nuclear Theory at the University of Washington for its hospitality and the US Department of Energy for partial support during the completion of this work. J. L.-A. thanks CERN Theory Division for kind hospitality, and Universidad de Córdoba and Ministerio de Cultura y Deporte of Spain (grant AP2001-3333) for financial support. C. A. S. is supported by a Marie Curie Fellowship of the European Community programme TMR (Training and Mobility of Researchers), under the contract number HPMF-CT-2000-01025.

References

- [1] M. Arneodo, Phys. Rept. **240**, 301 (1994).
- [2] D. F. Geesaman, K. Saito and A. W. Thomas, Ann. Rev. Nucl. Part. Sci. **45**, 337 (1995).
- [3] S. J. Brodsky, T. E. Close and J. F. Gunion, Phys. Rev. **D6**, 177 (1972); S. J. Brodsky and H. J. Liu, Phys. Rev. Lett. **64**, 1342 (1990).
- [4] N. N. Nikolaev and B. G. Zakharov, Z. Phys. **C49**, 607 (1991).
- [5] V. Barone, M. Genovese, N. N. Nikolaev, E. Predazzi and B. G. Zakharov, Z. Phys. **C58**, 541 (1993).

- [6] B. Z. Kopeliovich and B. Povh, Phys. Lett. **B367**, 329 (1996).
- [7] N. Armesto and M. A. Braun, Z. Phys. **C76**, 81 (1997).
- [8] N. Armesto, Eur. Phys. J. **C26**, 35 (2002).
- [9] B. Z. Kopeliovich, J. Raufeisen and A. V. Tarasov, Phys. Rev. **C62**, 035204 (2000); J. Nemchik, arXiv:hep-ph/0301043.
- [10] A. Capella, A. B. Kaidalov, C. Merino, D. Pertermann and J. Tran Thanh Van, Eur. Phys. J. **C5**, 111 (1998).
- [11] L. Frankfurt, V. Guzey, M. McDermott and M. Strikman, JHEP **0202**, 027 (2002); L. Frankfurt, V. Guzey and M. Strikman, arXiv:hep-ph/0303022.
- [12] L. V. Gribov, E. M. Levin and M. G. Ryskin, Phys. Rept. **100**, 1 (1983).
- [13] A. H. Mueller and J.-W. Qiu, Nucl. Phys. **B268**, 427 (1986); J.-W. Qiu, Nucl. Phys. **B291**, 746 (1987); E. L. Berger and J.-W. Qiu, Phys. Lett. **B206**, 42 (1988).
- [14] L. D. McLerran and R. Venugopalan, Phys. Rev. **D49**, 2233 (1994); 3352; **D50**, 2225 (1994).
- [15] A. H. Mueller, arXiv:hep-ph/0208278.
- [16] R. Venugopalan, Acta Phys. Polon. **B30**, 3731 (1999).
- [17] *QCD Perspectives on Hot and Dense Matter*, Eds. J.-P. Blaizot and E. Iancu, NATO Science Series, Kluwer Academic Publishers 2002.
- [18] N. Armesto and C. A. Salgado, Phys. Lett. **B520**, 124 (2001).
- [19] K. J. Eskola, V. J. Kolhinen and P. V. Ruuskanen, Nucl. Phys. **B535**, 351 (1998); K. J. Eskola, V. J. Kolhinen and C. A. Salgado, Eur. Phys. J. **C9**, 61 (1999).
- [20] D. Indumathi and W. Zhu, Z. Phys. **C74**, 119 (1997).
- [21] M. Hirai, S. Kumano and M. Miyama, Phys. Rev. **D64**, 034003 (2001).
- [22] Yu. L. Dokshitzer, Sov. Phys. JETP **46**, 641 (1977) [Zh. Eksp. Teor. Fiz. **73**, 1216 (1977)]; V. N. Gribov and L. N. Lipatov, Yad. Fiz. **15**, 781 (1972) [Sov. J. Nucl. Phys. **15**, 438 (1972)]; G. Altarelli and G. Parisi, Nucl. Phys. **B126**, 298 (1977).

- [23] V. N. Gribov, Sov. Phys. JETP **29**, 483 (1969) [Zh. Eksp. Teor. Fiz. **56**, 892 (1969)]; Sov. Phys. JETP **30**, 709 (1970) [Zh. Eksp. Teor. Fiz. **57**, 1306 (1969)].
- [24] V. N. Gribov, Sov. Phys. JETP **26**, 414 (1968) [Zh. Eksp. Teor. Fiz. **53**, 654 (1967)].
- [25] V. A. Abramovsky, V. N. Gribov and O. V. Kancheli, Yad. Fiz. **18**, 595 (1973) [Sov. J. Nucl. Phys. **18**, 308 (1974)].
- [26] A. Capella, E. G. Ferreiro, A. B. Kaidalov and C. A. Salgado, Nucl. Phys. **B593**, 336 (2001).
- [27] A. Capella, E. G. Ferreiro, A. B. Kaidalov and C. A. Salgado, Phys. Rev. **D63**, 054010 (2001).
- [28] A. Capella, A. B. Kaidalov and J. Tran Thanh Van, Heavy Ion Phys. **9**, 169 (1999).
- [29] A. Capella and D. Sousa, Phys. Lett. **B511**, 185 (2001).
- [30] C. W. De Jager, H. De Vries and C. De Vries, Atom. Data Nucl. Data Tabl. **14**, 479 (1974).
- [31] M. A. Preston and R. K. Bhoduri, *Structure of the nucleus*, Addison-Wesley, New York 1975.
- [32] K. Golec-Biernat and M. Wüsthoff, Phys. Rev. **D60**, 114023 (1999).
- [33] J. Breitweg *et al.* [ZEUS Collaboration], Eur. Phys. J. **C1**, 81 (1998).
- [34] J. Breitweg *et al.* [ZEUS Collaboration], Eur. Phys. J. **C2**, 237 (1998).
- [35] A. Schwimmer, Nucl. Phys. **B94**, 445 (1975).
- [36] M. R. Adams *et al.* [E665 Collaboration], Z. Phys. **C67**, 403 (1995).
- [37] M. R. Adams *et al.* [E665 Collaboration], Phys. Rev. Lett. **68**, 3266 (1992).
- [38] M. Arneodo *et al.* [NMC Collaboration], Nucl. Phys. **B481**, 3 (1996).
- [39] P. Amaudruz *et al.* [NMC Collaboration], Nucl. Phys. **B441**, 3 (1995).
- [40] M. Arneodo *et al.* [NMC Collaboration], Nucl. Phys. **B481**, 23 (1996).

- [41] N. Armesto, A. Capella, A. B. Kaidalov, J. López-Albacete and C. A. Salgado, in preparation.
- [42] Z. Huang, H. J. Lu and I. Sarcevic, Nucl. Phys. **A637**, 79 (1998).
- [43] J. Bartels, E. Gotsman, E. M. Levin, M. Lublinsky and U. Maor, arXiv:hep-ph/0304166.
- [44] K. J. Eskola, H. Honkanen, V. J. Kolhinen and C. A. Salgado, arXiv:hep-ph/0302170.
- [45] E. Gotsman, E. M. Levin, M. Lublinsky and U. Maor, Eur. Phys. J. **C27**, 411 (2003).
- [46] M. Arneodo *et al.*, in *Proceedings of the Workshop on Future Physics at HERA* (Hamburg, Germany, September 1995); H. Abramowicz *et al.*, in *TESLA Technical Design Report, Part VI, Chapter 2*, Eds. R. Klanner, U. Katz, M. Klein and A. Levy; *EIC White Paper*, preprint BNL-68933, Eds. A. Deshpande, R. Milner and R. Venugopalan.
- [47] F. P. Schilling [H1 Collaboration], arXiv:hep-ex/0210027.
- [48] C. Adloff *et al.* [H1 Collaboration], Z. Phys. **C76**, 613 (1997).
- [49] L. Caneschi, A. Schwimmer and R. Jengo, Nucl. Phys. **B108**, 82 (1976); S. Bon-darenko, E. Gotsman, E. M. Levin and U. Maor, Nucl. Phys. **A683**, 649 (2001).
- [50] A. Capella, A. B. Kaidalov, C. Merino and J. Tran Thanh Van, Phys. Lett. **B343**, 403 (1995); A. Capella, A. B. Kaidalov, C. Merino, D. Pertermann and J. Tran Thanh Van, Phys. Rev. **D53**, 2309 (1996).
- [51] Proceedings of the *XVIth International Conference On Ultrarelativistic Nucleus-Nucleus Collisions: Quark Matter 2002 (QM 2002)* (Nantes, France, 18-24 July 2002), to appear in Nucl. Phys. **A**.
- [52] N. Armesto and C. Pajares, Int. J. Mod. Phys. **A15**, 2019 (2000).

Figure captions:

Fig. 1. Diagram showing diffractive DIS with the corresponding kinematical variables in the infinite momentum frame (left) and its equivalence in the rest frame of the nucleon (right).

Fig. 2. Diagram showing the equivalence between diffractive DIS and two exchanged amplitudes with a cut between the amplitudes.

Fig. 3. Results of the model using Schwimmer (solid lines) and eikonal (dashed lines) unitarization compared with experimental data versus x , for the ratios C/D, Ca/D, Pb/D [36] and Xe/D [37] (filled circles correspond to the analysis with hadron requirement and open circles to that with electromagnetic cuts, see the experimental paper for more details).

Fig. 4. Results of the model using Schwimmer (open circles) and eikonal (open triangles) unitarization compared with experimental data versus A , for the ratios Be/C, Al/C, Ca/C, Fe/C, Sn/C and Pb/C [38] at two fixed values of x .

Fig. 5. Id. to Fig. 3 but for the ratios He/D, C/D and Ca/D [39].

Fig. 6. Results of the model using Schwimmer (solid lines) and eikonal (dashed lines) unitarization compared with experimental data versus Q^2 , for the ratio Sn/C [40] at two fixed values of x .

Fig. 7. Comparison of the results of our model using Schwimmer (solid lines) and eikonal (dashed lines) unitarization for the ratio Pb/nucleon with other models, versus x at fixed $Q^2 = 3$ GeV 2 . HKM are the results from [21], Sarcevic from [42], Bartels from [43], Frankfurt from [11] (at $Q^2 = 4$ GeV 2), Armesto from [8] and EKS98 from [19].

Fig. 8. Results of the model using Schwimmer (solid lines) and eikonal (dashed lines) unitarization for the ratios D/nucleon, He/nucleon, Li/nucleon, C/nucleon, Ca/nucleon, Sn/nucleon and Pb/nucleon versus x at $Q^2 = 0.5, 2$ and 5 GeV 2 .

Fig. 9. Results of the model for $Q^2 = 0$ using Schwimmer (solid lines) and eikonal (dashed lines) unitarization for the ratios D/nucleon, He/nucleon, Li/nucleon, C/nucleon, Ca/nucleon, Sn/nucleon and Pb/nucleon (upper plot), and for different impact parameters b for the ratios C/nucleon (plot in the middle) and Pb/nucleon (lower plot), versus

W^2 .

Fig. 10. Results for $Q^2 = 0.5$ (upper plot) and 5 (lower plot) GeV^2 using Schwimmer unitarization for the ratio Pb/nucleon versus x , of the model without modifications (solid lines), without the higher-twist contribution in the short-distance component (dashed lines), and without the higher-twist contribution in the short-distance component plus some modification in parameters (dotted lines) to check the sensibility of the results, see text.

Fig. 11. Diagram showing the contribution to particle production in the central region in AB collisions.

Fig. 12. Results of the model for the multiplicity reduction factor versus impact parameter b at $y^* = 0$, for AuAu collisions at $\sqrt{s} = 19, 130$ and 200 GeV per nucleon, and for PbPb collisions at $\sqrt{s} = 5500$ GeV per nucleon, in the parton model-like realization (solid lines) and for $[C = 0.31 \text{ fm}^2, \Delta = 0.13]$ (dashed lines).

Fig. 13. Id. to Fig. 12 but for AuAu collisions at $\sqrt{s} = 200$ GeV per nucleon and for PbPb collisions at $\sqrt{s} = 5500$ GeV per nucleon, for $y^* = 1, 2$ and 3 .

Fig. 14. Results of the model for the multiplicity reduction factor versus impact parameter b at $y^* = 0$, for AuAu collisions at $\sqrt{s} = 200$ GeV per nucleon, in the parton model-like realization (upper plot) and for $[C = 0.31 \text{ fm}^2, \Delta = 0.13]$ (lower plot). In each plot, lines from bottom to top correspond to $m_T^2 = 0.16, 1, 2, 3, 4$ and 5 GeV^2 .

Figures:

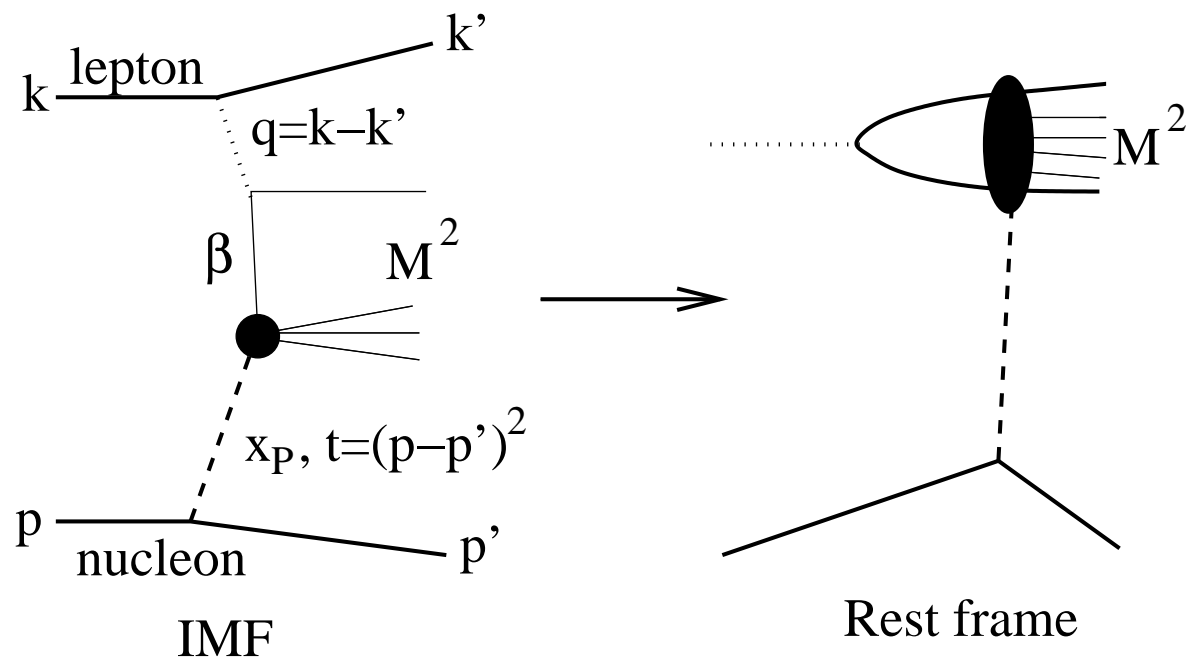


Fig. 1

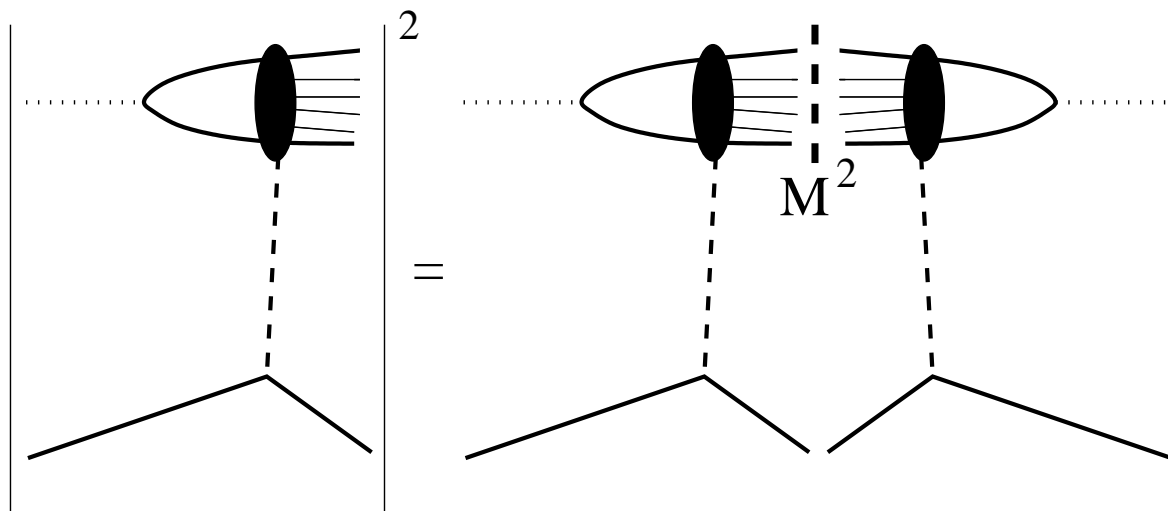


Fig. 2

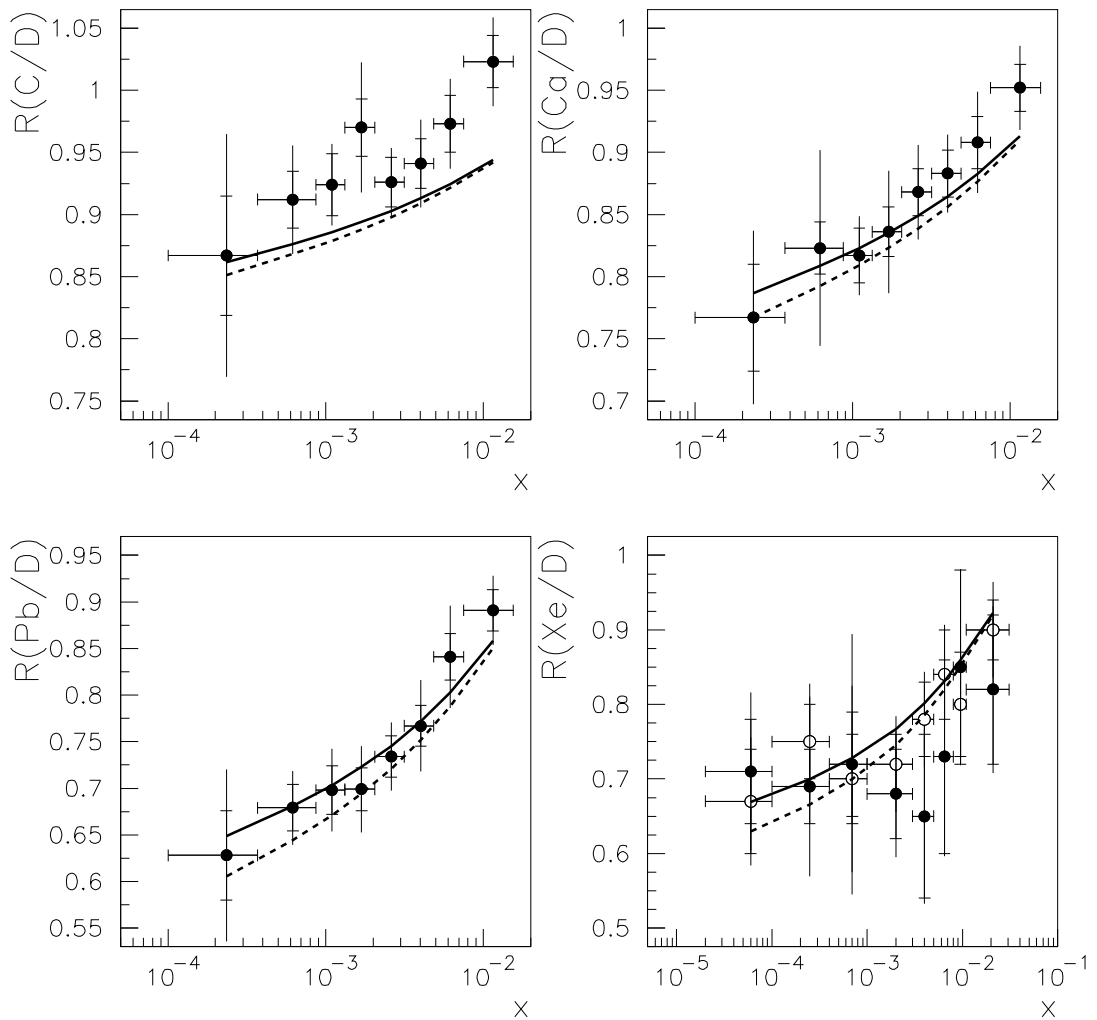


Fig. 3

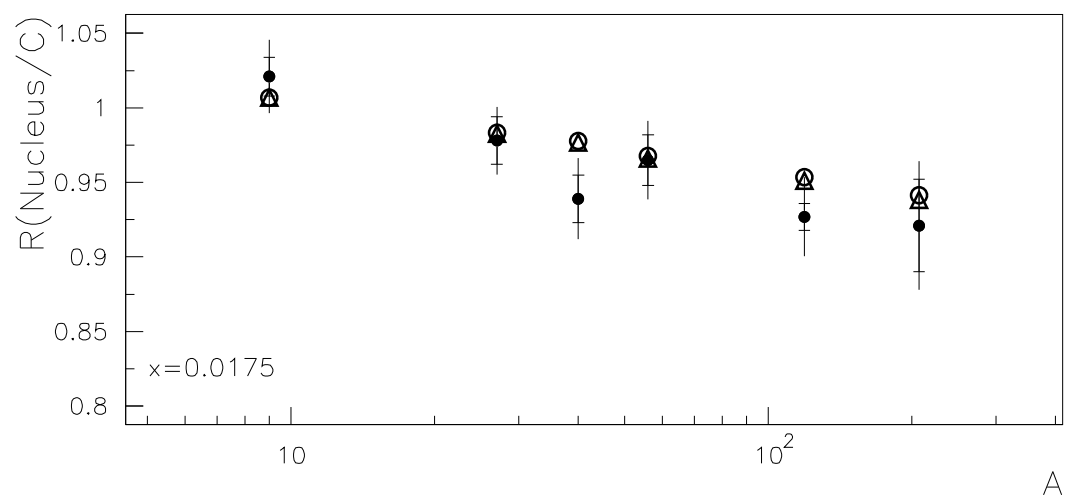
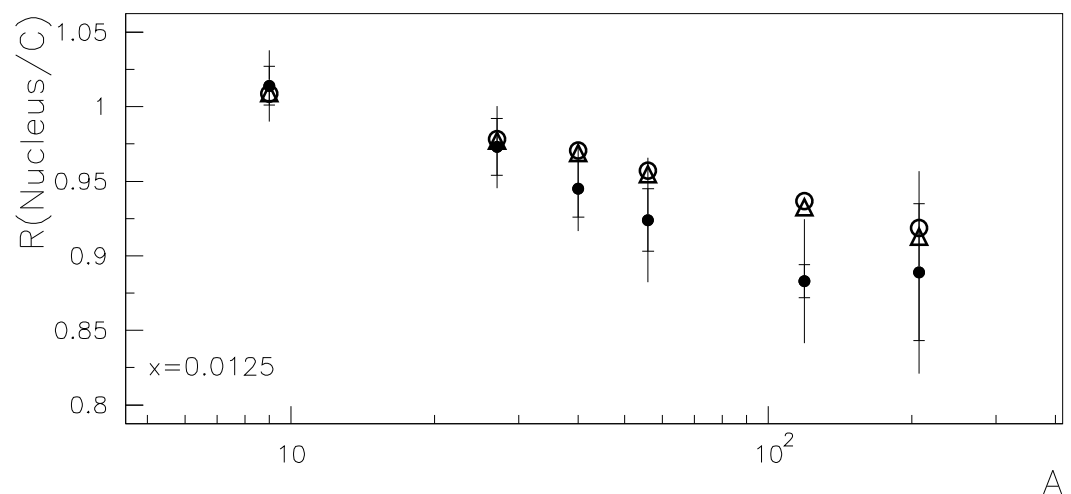


Fig. 4

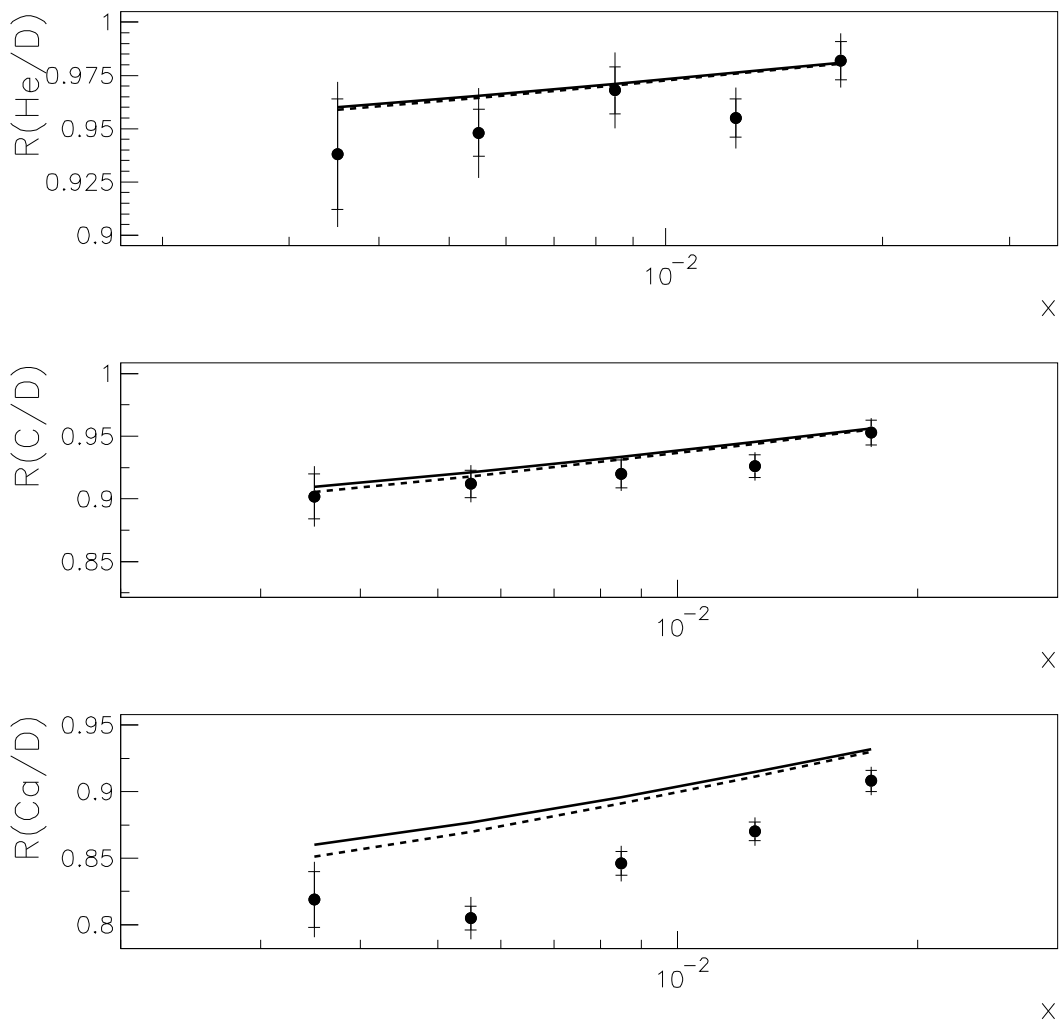


Fig. 5

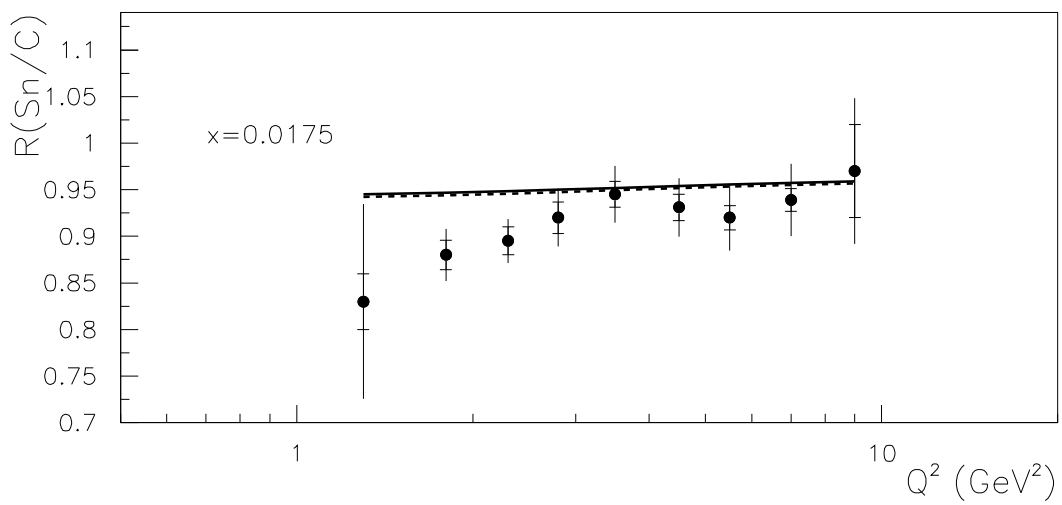
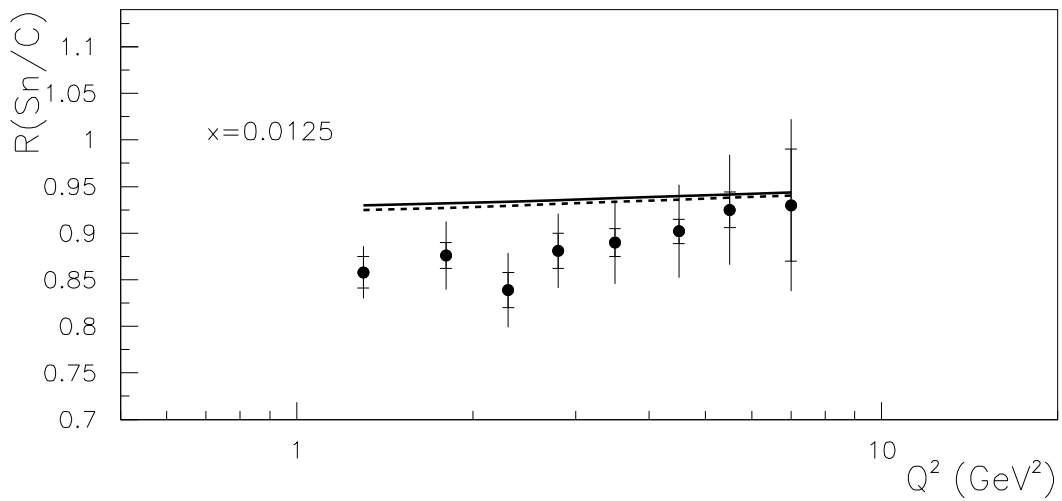


Fig. 6

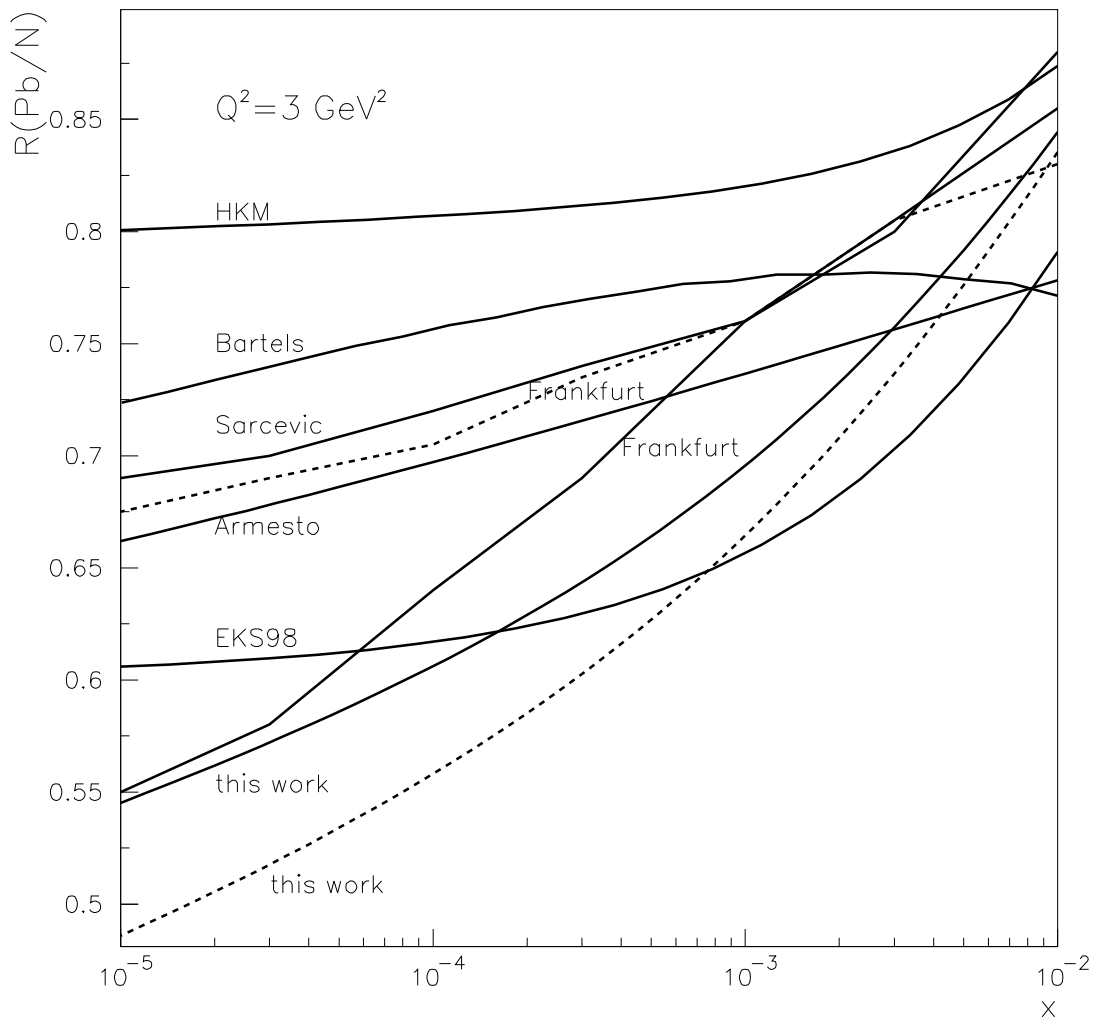


Fig. 7

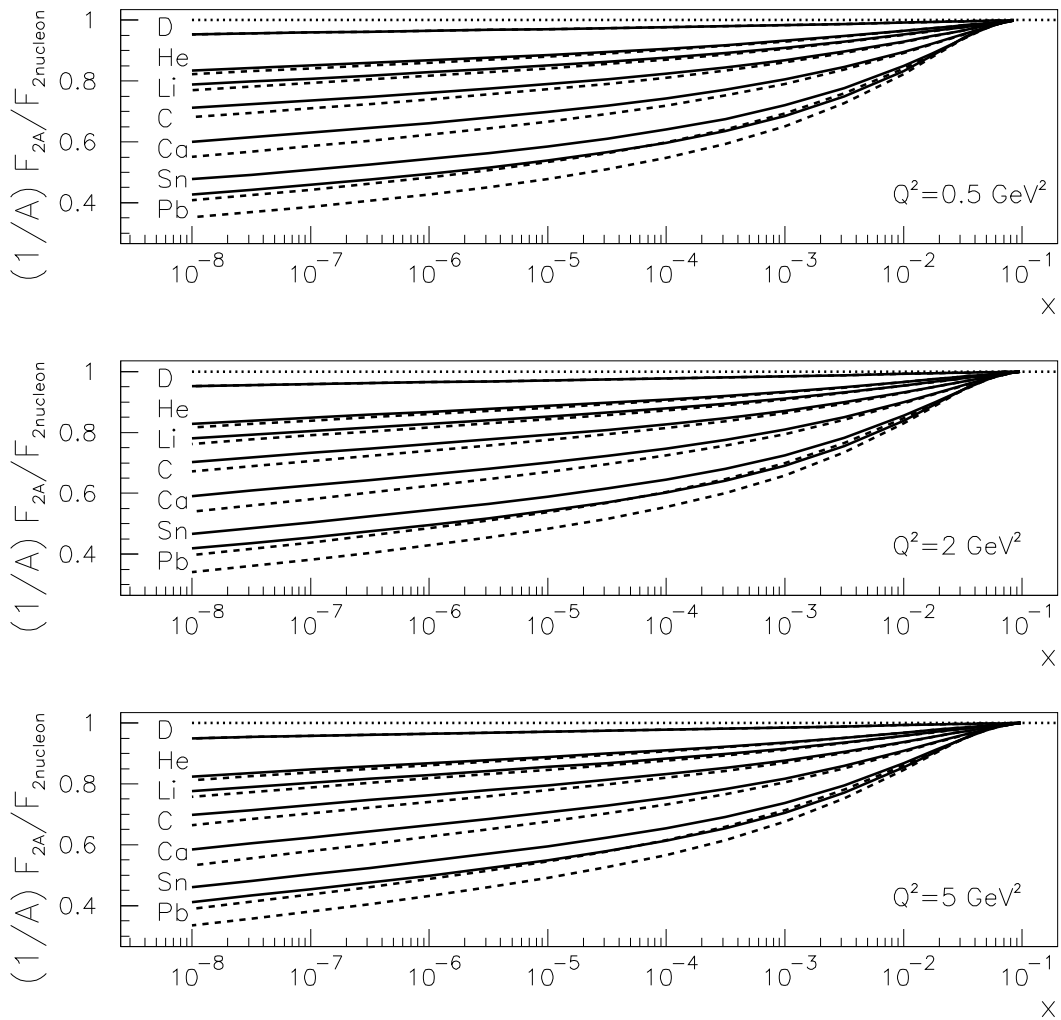


Fig. 8

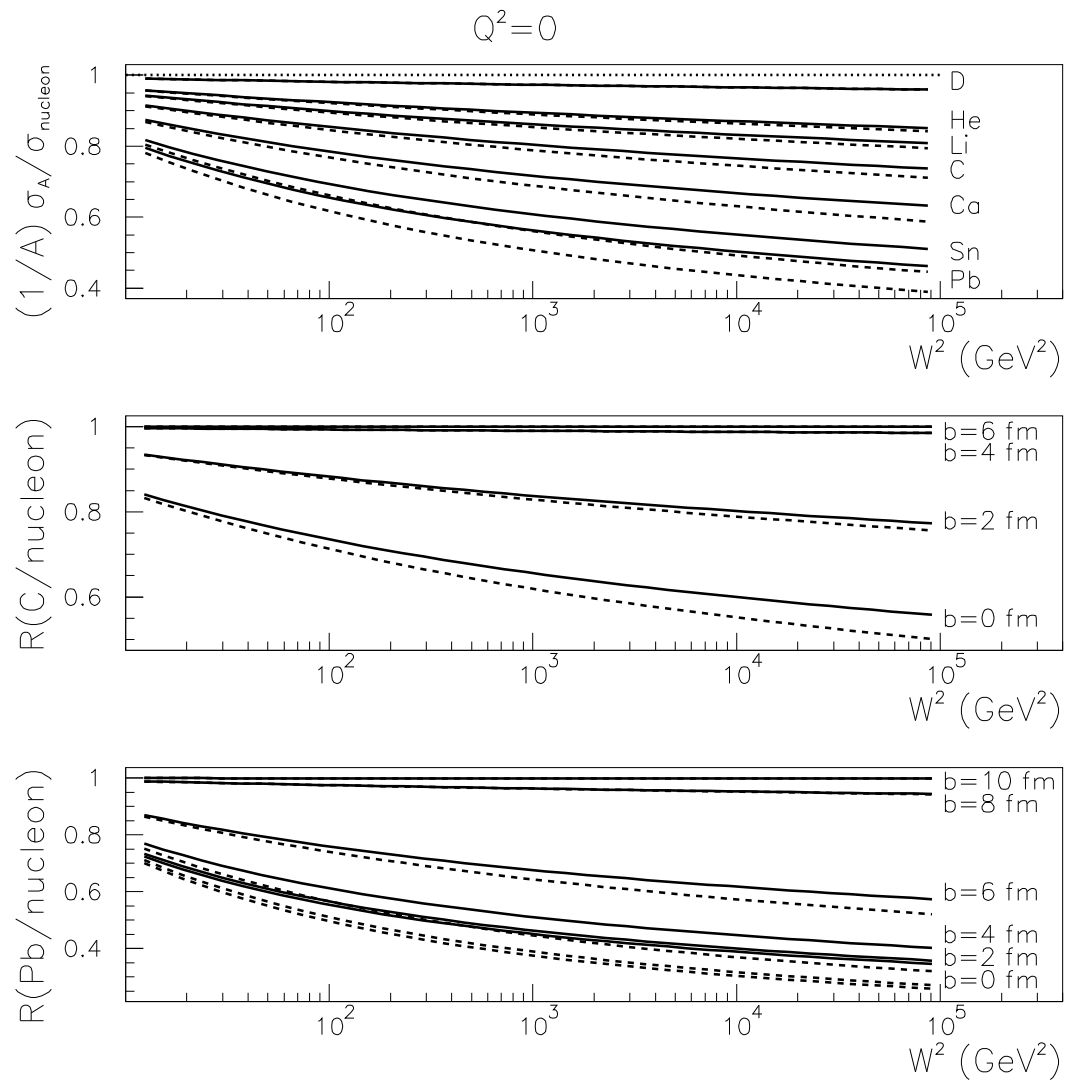


Fig. 9

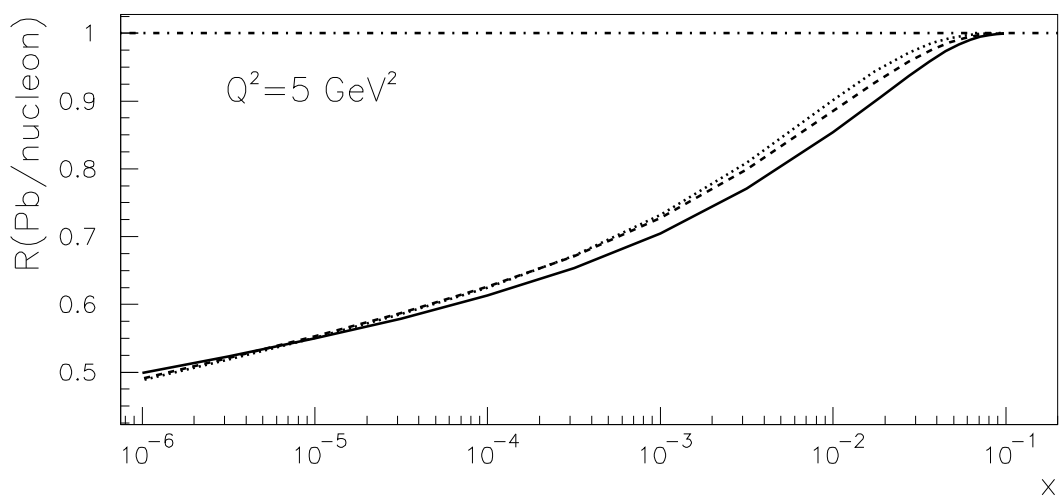
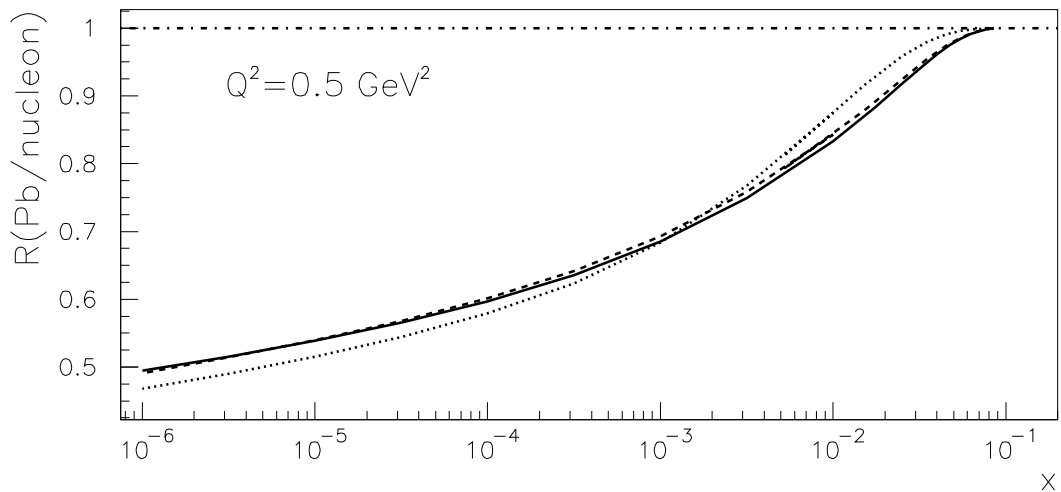


Fig. 10

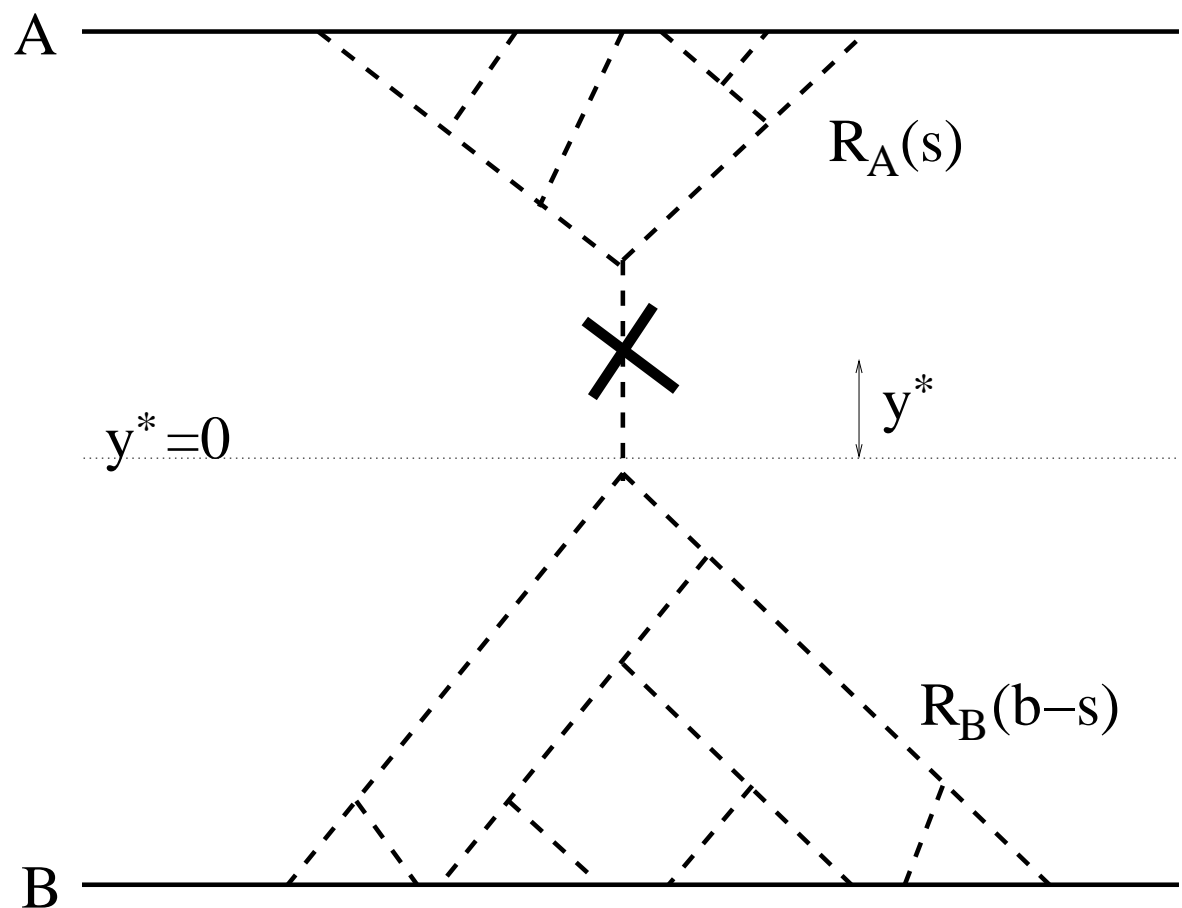


Fig. 11

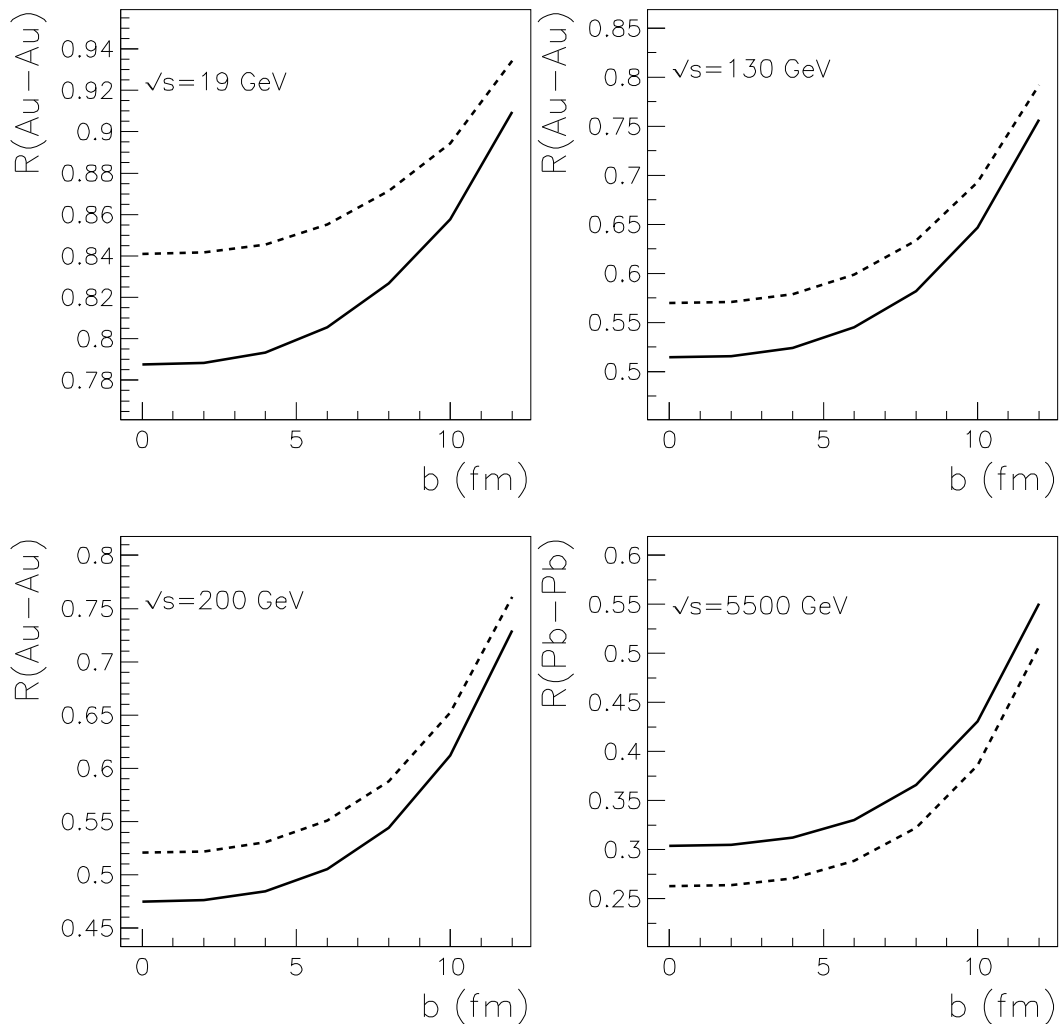


Fig. 12

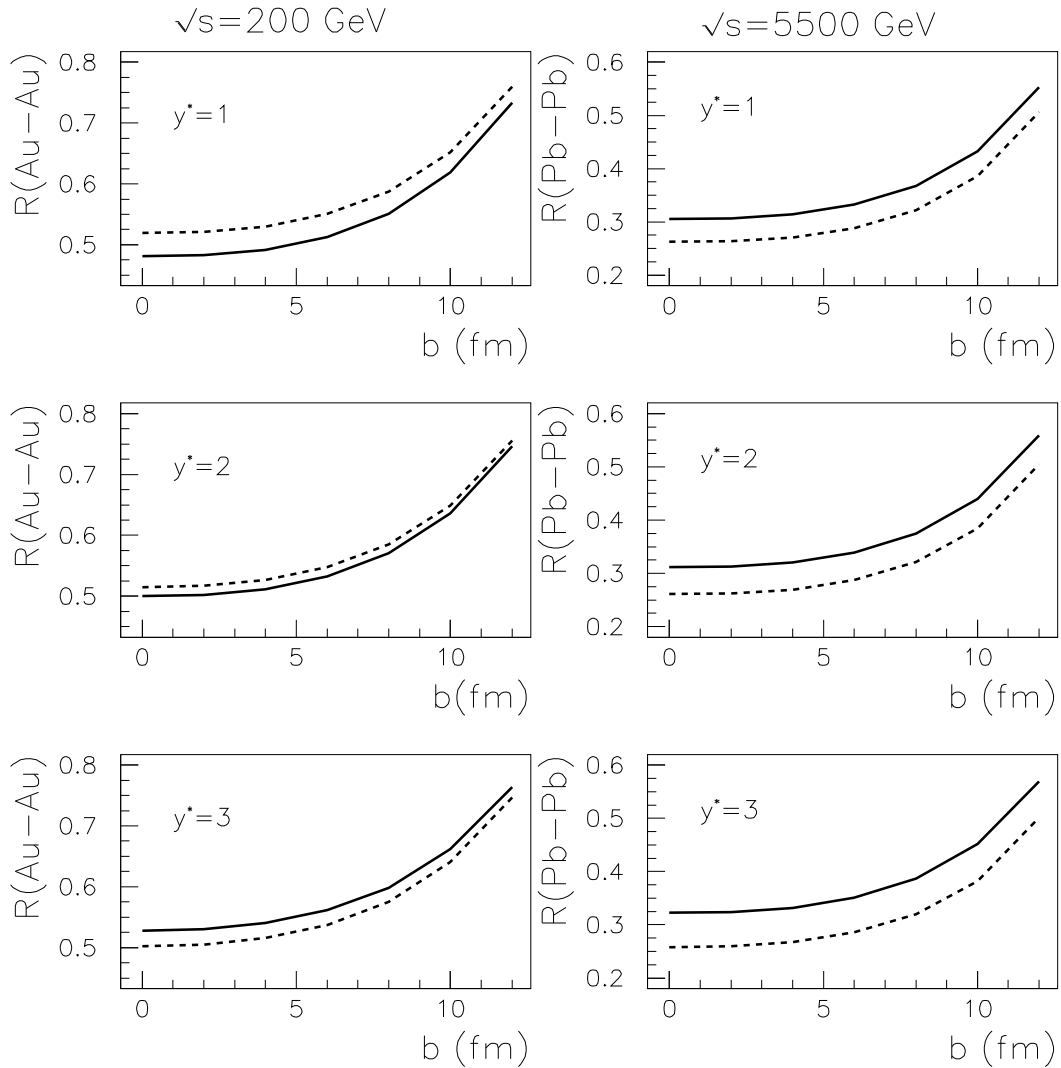


Fig. 13

parton model-like

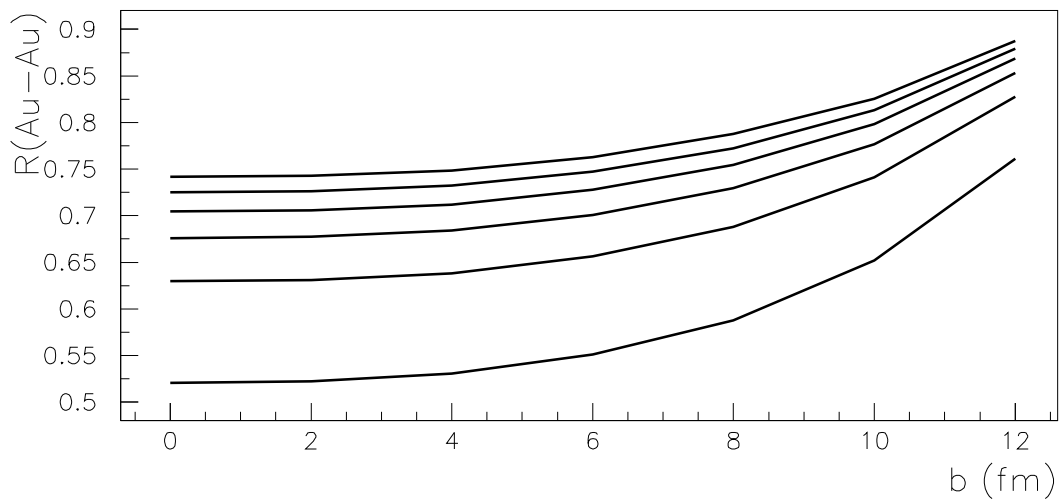
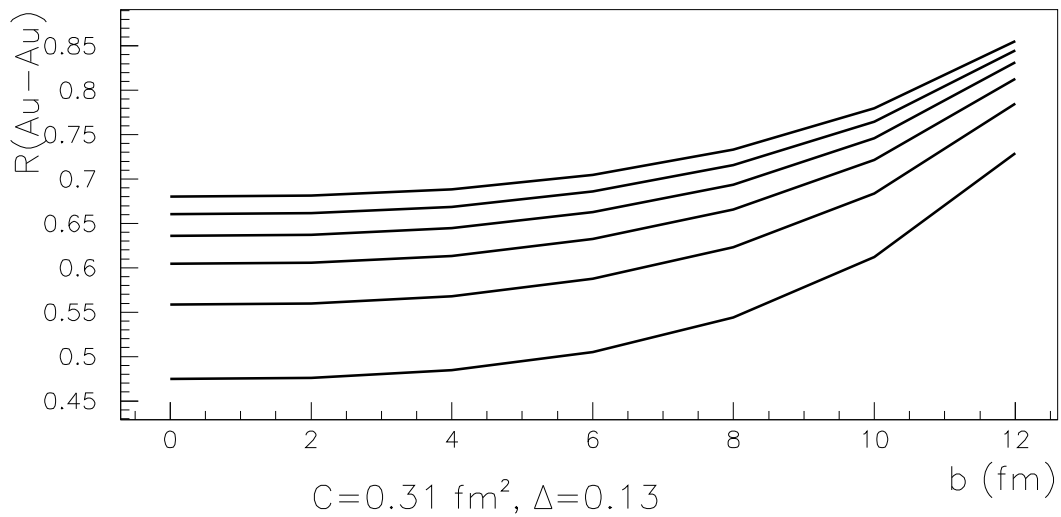


Fig. 14